

Infrared Spectroscopic Observations of the Secondary Stars of Short Period Sub-Gap Cataclysmic Variables

Ryan T. Hamilton, Thomas E. Harrison

New Mexico State University

Department of Astronomy, PO Box 300001, MSC 4500, Las Cruces, NM 88003

rthamilt@nmsu.edu, tharriso@nmsu.edu

and

Claus Tappert

Universidad de Valparaiso

Valparaiso, Chile

ctappert@astro.puc.cl

and

Steve B. Howell

NOAO

950 N. Cherry Avenue, Tucson, AZ 85726

howell@noao.edu

Received _____; accepted _____

ABSTRACT

We present K -band spectroscopy of short period, “sub-gap” cataclysmic variable (CV) systems obtained using ISAAC on the VLT. We show the infrared spectra (IR) for nine systems below the 2-3 hour period gap: V2051 Oph, V436 Cen, EX Hya, VW Hyi, Z Cha, WX Hyi, V893 Sco, RZ Leo, and TY PsA. We are able to clearly detect the secondary star in all but WX Hyi, V893 Sco, and TY PsA. We present the first direct detection of the secondary stars of V2051 Oph, V436 Cen, and determine new spectral classifications for EX Hya, VW Hyi, Z Cha, and RZ Leo. We find that the CO band strengths of all but Z Cha appear normal for their spectral types, in contrast to their longer period cousins above the period gap. This brings the total number of CVs and pre-CVs with moderate resolution ($R \gtrsim 1500$) IR spectroscopy to sixty-one systems: nineteen pre-CVs, thirty-one non-magnetic systems, and eleven magnetic or partially magnetic systems. We discuss the trends seen in the IR abundance patterns thus far, and highlight a potential link between anomalous abundances seen in the IR with the C IV/N V anomaly seen in the ultraviolet. We present a compilation of all systems with sufficient resolution IR observations to assess the CO band strengths, and, by proxy, obtain an estimate on the C abundance on the secondary star.

Subject headings: cataclysmic variables — infrared: stars — stars: abundances

1. Introduction

Cataclysmic variables (CVs) are short-period binaries in which a late-type, Roche-lobe filling secondary star transfers matter through an accretion disk onto a rotating, accretion heated primary white dwarf (WD). The standard evolutionary paradigm (Howell et al. 2001, hereafter HNR) postulates that CVs evolve from wide binaries of moderate orbital period and unequal masses. As the more massive component evolves off of the main sequence into a red giant, the secondary star finds itself orbiting within the atmosphere of the massive star. During this common envelope phase, the orbit of the secondary star shrinks due to interactions with the atmosphere of the more massive primary star. This shortens the binary period, until the common envelope is ejected around orbital periods of 1 day. Angular momentum is then mainly lost through an efficient magnetically constrained wind, (“magnetic braking”, see Collier Cameron 2002, and references therein), shrinking the orbit so much that the Roche lobe of the secondary star comes into contact with the stellar surface and mass transfer begins, signaling the birth of a long period CV. As the system evolves, the secondary star continues to lose mass, but angular momentum losses keep the secondary star in contact with its Roche lobe.

During their lives as longer period CVs, orbital periods typically range from 3 to 10 hours, and mass transfer rates from 10^{-8} to $10^{-9} M_{\odot}\text{yr}^{-1}$. This rapid mass transfer drives the secondary star out of thermal equilibrium, causing it to become bloated by $\sim 30\%$ compared to an isolated star at the same mass (Knigge 2006). The secondary continues to lose mass until it reaches the fully convective boundary ($P_{\text{orb}} \approx 3$ hrs, $M_2 \approx 0.2 - 0.3 M_{\odot}$), where the magnetic braking is believed to be disrupted. The secondary star is able to regain its thermal equilibrium, and as a result shrinks and loses contact with its Roche lobe ceasing mass transfer. With the disruption of magnetic braking from the secondary star, angular momentum in the system is lost via gravitational radiation alone, causing the orbit

to decrease at a much slower rate. This continues until the orbit has shrunk sufficiently for the secondary star to overflow its Roche lobe and begin mass transfer once again ($P_{\text{orb}} \approx 2$ hrs). With the absence of mass transfer between orbital periods of 2-3 hours, the systems are dormant, and consequently, difficult to identify. This forms a gap in the observed orbital period distribution of CVs between 2-3 hours. Once mass transfer resumes, the system emerges as a “sub-gap” CV.

It is assumed that this evolutionary sequence happens on a short enough timescale that the secondary star does not undergo any significant nuclear evolution, and therefore should retain normal abundance patterns consistent with a main sequence dwarf. Observational evidence, however, shows a growing number of systems with apparent abundance anomalies seen in the UV and/or the IR; in the UV, this is seen as unusual N V/C IV ratios (Gänsicke et al. 2005), and in IR, this is inferred through the presence of anomalously weak or absent CO features.

Harrison et al. (2004b, 2005a,b) show that for thirteen out of the nineteen systems observed, the CO features of non-magnetic CVs above the period gap are much weaker than they should be for their spectral types. Since the water vapor features in the coolest of these stars appears normal, this result points towards a deficit of carbon. In addition, ^{13}C appeared to be enhanced for several systems, an indication of CNO processed material in the atmosphere of the secondary star (Harrison et al. 2004b). In contrast to these non-magnetic CVs above the gap, the majority (8/11 systems) of “polars”, CVs with highly magnetic WD primaries, have secondary stars that appear to be completely normal (Harrison et al. 2005a, 2007). Pre-CV systems appear uniformly normal, with only one of nineteen systems showing any weakened CO features (Tappert et al. 2007; Howell et al. 2010). While the total CV sample is somewhat small and limited to the brightest objects observable with ground-based near-IR spectroscopic instrumentation, these trends are striking enough to

warrant further attention and examination of all CV subtypes.

Observations of short period, sub-gap CVs are extremely challenging given the very low luminosities expected for the secondary stars that must compete against that of accretion and the underlying hot white dwarf. IR spectroscopy of CVs has been possible since the early 1990's, notably with the efforts of Dhillon & Marsh (1995) looking at systems well above the 2-3 hour period gap, where absorption lines from the secondary were clearly seen. Dhillon et al. (2000) observed five systems below the period gap, and found that the secondary stars were too faint to detect and estimated that they contribute only 10 to 30% to the observed infrared flux.

Mennickent et al. (2004) and Mennickent & Diaz (2002) focused on lower resolution studies of sub-gap systems, fitting K or M dwarf template spectra to low resolution optical and near-IR spectra. This technique was employed by Ishioka et al. (2007) who used the Subaru Telescope to obtain J , H , and K -band low resolution grism spectroscopy of five CVs below the gap. Spectral component fitting allowed them to obtain rough spectral type estimates ranging from M1 to L1, but the low resolution of these data (FWHM $\sim 60\text{\AA}$) prevented examination of the CO features.

To attempt to detect the secondary stars in a sample of sub-gap CVs, we have obtained moderate resolution K -band spectra of nine systems. This increases the sample of CVs with moderate resolution ($R \gtrsim 1500$) near-IR spectroscopy to sixty-one systems: nineteen pre-CVs, thirty-one non-magnetic systems, and eleven magnetic or partially magnetic systems. Prior to this work, three quarters of the non-magnetic systems were *above* the period gap and only four below: RZ Leo, WZ Sge, GW Lib, and EI Psc. Howell et al. (2010) presented the K -band spectrum of RZ Leo, which showed no evidence of a C deficit manifested as weakened or absent CO features. Harrison et al. (2009) obtained moderate resolution observations VY Aqr and EI Psc, finding evidence for strong deficits of C in

both systems. Howell et al. (2004) presented observations of WZ Sge, showing this object to have both CO and H₂ emission from its accretion disk, the only such detection so far.

In our nine observed systems, we clearly detect the presence of the secondary star in six of them. In two of the remaining cases, we are able to provide constraints on their spectral types, and in only one system we could not detect the signature of the secondary star. In contrast to the longer period CVs, the majority of these secondary stars have CO features that appear to be present at near-normal strengths. We present our observations in §2, the object spectra and spectral type determinations in §3, a discussion of our results in §4, and our conclusions in §5.

2. Observations

Infrared spectroscopy for the program objects was carried out at the European Southern Observatory (ESO) at Cerro Paranal, Chile, with the Infrared Spectrometer And Array Camera (ISAAC) (Moorwood et al. 1998) on the 8.2 meter Very Large Telescope (VLT) Antu in service mode between May and August of 2008. Additional infrared data were obtained for both RZ Leo and EX Hya utilizing NIRSPEC (McLean et al. 1998) at the W. M. Keck Observatory on Mauna Kea. An observation log describing the observations is presented in Table 1, listing the observation dates and times for each system, the exposure times, the number of observations at each nodded position, and the percentage of the orbital phase covered by the observations.

2.1. VLT Antu

The ISAAC data were obtained in the standard infrared ABBA nodding pattern, moving the object between two positions on the spectrograph slit to aid in the removal of

sky background. These data were taken using the medium resolution grating and a $0.6''$ slit, giving a resolving power of $R \sim 4400$ and a dispersion of $1.20 \text{ \AA pixel}^{-1}$ across the 1024 pixel square ISAAC science CCD. We used two wavelength centers (2.25 and $2.35 \mu m$) giving sufficient overlap to construct a composite spectrum covering 2.18 to $2.40 \mu m$. The observing conditions varied during the observation period but, in general, these data were obtained in fair conditions with seeing generally less than $1.25''$ as reported by the Differential Image Motion Monitor (DIMM) at the VLT.

Several problems appeared during the observation run, however, that affected the quality of these data. Several large dust particles appeared on the detector, degrading the cosmetics and compromising the spectral extraction. This specifically impacted the data for V436 Cen and V893 Sco. In addition, significant drift in the central wavelength positions were observed, particularly if the center position was changed before, or after, a telluric standard was observed. Using night sky lines as a wavelength calibration source mitigated this effect, but in general telluric correction and wavelength calibration were more challenging than expected. The final spectra for our program objects are shown in Fig. 1.

2.2. Keck Observatory

Both EX Hya and RZ Leo were observed using NIRSPEC at the W. M. Keck Observatory, using a $0.380''$ slit and a low resolution grating covering approximately 2.04 to $2.46 \mu m$ with a dispersion of $4.27 \text{ \AA pixel}^{-1}$. These data were obtained in the standard infrared ABBA nodding pattern, and reduced using the IDL routine REDSPEC¹. The data reduction process followed the description given in Harrison et al. (2005a). Both objects had telluric corrections applied in REDSPEC using observations of featureless A0V stars close to the program objects to remove atmospheric absorption lines, and to avoid any differences in telluric absorption dependent on airmass. We used arc lamps to provide

a wavelength calibration. The spectrum for RZ Leo has been presented in Howell et al. (2010), but we include it here to compare it to our results for the other sub-gap systems in Fig. 1.

2.3. Reductions

Standard data reductions of the VLT data were carried out using ESO GASGANO² interface and the Common Pipeline Library (CPL) using the ISAAC reduction recipes version 5.7.0. The pipeline obtains a wavelength calibration by examining the night sky lines in each data frame, and corrects for field curvature using arc lamp frames collected at the end of each night as well as dividing by a flat field. It then detects the spectrum present in each input frame, shifting and co-adding to produce a single output spectrum. Modifications were made to this pipeline to output the individual corrected frames, which could then be properly combined after the reduction process to account for the significant radial velocity motions of the secondary star. While we were able to obtain a well corrected spectrum for each system, the resulting radial velocity curves were extremely noisy and are not presented here. The modifications to the CPL recipes were checked for accuracy by also examining the data with standard IRAF³ methods (*APALL*, *IDENTIFY*, etc.) and found to give indistinguishable results. Telluric features were removed using nearby A0V standard stars observed close to the same airmass as the program objects. Telluric standard stars were in general observed at the end of each night, within ± 0.2 airmasses of the program objects. In most cases only one telluric standard was observed each night. These followed the same reduction process as the data frames, but instead used the single combined

¹Details about the REDSPEC IDL package can be found on-line at the instrument website at <http://www2.keck.hawaii.edu/inst/nirspec/redspeg.html>.

output from the reduction pipeline since radial velocity smearing was not an issue. The most appropriate standard was then divided into the observation using the IRAF task *TELLURIC*, which allows scaling and shifting the standard to best match the atmospheric absorption lines present in the data. Care was taken to not scale or shift the standard too much and introduce spurious absorption or emission lines to our program object spectra.

2.4. M Star Templates

In addition to the spectra of the CVs, we obtained spectra of three late-type dwarf templates: LHS 427, LHS 2347, and LHS 3003. Each reference object was compared against standards taken from the IRTF Spectral Library (Cushing et al. 2005) as a check on the spectral reductions, and the spectral types we derive are consistent with those reported in the SIMBAD database. The observing log of the M stars observed as part of our program can be found in Table 1. When necessary, these three M star templates were supplemented with additional, lower resolution ($R \sim 2,000$) spectra from the IRTF Spectral Library for comparison purposes.

3. Results

In the following, we attempt to assign spectral types to the secondary stars of our program objects if they are clearly visible. The Ca I triplet at $2.263 \mu m$ and the Na I

²<http://www.eso.org/sci/data-processing/software/gasgano/>

³IRAF is distributed by the National Optical Astronomy Observatories, which are operated by the Association of Universities for Research in Astronomy, Inc., under cooperative agreement with the National Science Foundation

doublet at $2.207 \mu m$ are good indicators of effective temperature (Ivanov et al. 2004, and references therein), thus we use both as an indication of spectral type. As the effective temperature decreases from M0, the Na I doublet gets stronger and the Ca I triplet gets weaker. The accretion disks in these systems are bright, and provide a flat power-law continuum that veils the absorption lines from the secondary star making a direct visual comparison to template spectral types as described in §2.4 more difficult. To overcome this, prior work (Mennickent & Diaz 2002; Mennickent et al. 2004; Ishioka et al. 2007) has focused on component fitting a range of stellar template spectra with a variable power law component to represent contributions from the disk to the J, H , and/or K band observations.

As a prelude to more in-depth synthetic spectral modeling currently underway, we take a very simplistic, yet effective, approach to get first estimates of the spectral types of the secondary stars visible in these data. The visible features in each object spectrum were enhanced using the IRAF task *SARITH* to raise the spectrum to some constant power, and then fit from 2.18 to $2.28 \mu m$ with a linear function using *CONTINUUM* to remove the overall continuum slope. We do not fit the continuum over the entire spectral range because of the presence of broad CO bands and changes in the continuum shape due to the onset of strong water vapor absorption past $\lambda \gtrsim 2.28 \mu m$, both noted by Tappert et al. (2007). The very broad H₂O features depress the continuum, especially in later spectral types, making it difficult to ascertain its true level in the continuum fitting process. The region between the Na I doublet and the Ca I triplet, our primary spectral type indicators, is relatively free of other contaminating sources, so we are confident that the lines are undistorted by this process. These object spectra are then compared by eye to the IRTF spectral templates described in §2.4. The high accretion disk contamination and low S/N of some of these data lead us to conclude that this approach was the best for determining the spectral types of these secondary stars.

3.1. V2051 Oph

V2051 Oph ($P_{\text{orb}} = 1.50$ hr) is an SU UMa type CV, exhibiting super-outbursts approximately every 227 days. It is also an eclipsing system, and was observed by Baptista et al. (1998) using both ground based photometry as well as *HST* FOS spectroscopy. They derived a secondary mass of $M_2 = 0.15 \pm 0.03 M_{\odot}$, and a radius of $R_2 = 0.16 \pm 0.01 R_{\odot}$, but make no estimate of the secondary spectral type. They do speculate, however, that the system must be relatively young since the secondary does not seem to be out of thermal equilibrium. The empirical CV donor sequence by Knigge (2006) suggests, assuming a solar composition, that the secondary star of V2051 Oph should have a spectral type near M7. The 2MASS Point Source Catalog (Skrutskie et al. 2006) lists V2051 Oph as having $K_{2\text{MASS}} = 13.53$.

The ISAAC spectrum of V2051 Oph is presented in Fig. 2. This spectrum shows that the first overtone CO feature is stronger than the Na I doublet, suggesting a very late spectral type. The Ca I triplet is also not clearly detected, as would be expected if the secondary had a late-M spectral type. From comparison of its spectrum to the templates we derive a spectral type of $M7 \pm 1$ for V2051 Oph. The secondary of V2051 Oph has not been previously detected, thus this *K*-band spectrum provides the first direct constraint on its spectral type.

3.2. V436 Cen

V436 Cen ($P_{\text{orb}} = 1.50$ hr) is an SU UMa type CV, exhibiting super-outbursts approximately every 630 days. It has been suggested (Patterson 2001) that V436 Cen could harbor a low mass secondary based on empirical fits to a relationship between the mass ratio q and the superhump and orbital periods. In quiescence, V436 Cen has $K_{2\text{MASS}} = 13.53$.

Ritter & Kolb (2003, update 7.12) report a secondary mass of $M_2 = 0.17 M_\odot$, but list it as uncertain. It is interesting to note how similar V2051 Oph and V436 Cen are in terms of orbital period, M_2 , and even $K_{2\text{MASS}}$, which all would imply that the secondary star of V436 Cen should be very much like that of V2051 Oph, an M7 dwarf donor.

The spectrum of V436 Cen, shown in Fig. 2, appears to be slightly later than that of V2051 Oph. Using the Na I, Ca I, and CO features we derive a spectral type of $M8 \pm 1$. The data reduction process for this object was somewhat hampered by the lack of a good telluric standard to correct its spectra. As with V2051 Oph, this is the first direct detection of the secondary in V436 Cen.

3.3. EX Hya

EX Hya is a bright ($K_{2\text{MASS}} = 11.69$), well studied short period ($P_{\text{orb}} = 1.64$ hr) Intermediate Polar (IP), and is the only magnetic CV in our sample. Beuermann & Reinsch (2008) used optical spectroscopy and a previously derived value of K_1 , finding the mass of the secondary to be $M_2 = 0.108 \pm 0.008 M_\odot$, with a radius of $R_2 = 0.1516 \pm 0.0034 R_\odot$. They assigned a spectral type of $M5.5 \pm 0.5$ on the basis of Na I and TiO band strengths compared to M4V and M6V templates. *JHK* spectra of EX Hya during outburst were presented by Harrison et al. (2010a), who noted that both water vapor absorption (at 1.38 and 1.9 μm) and the Na I doublet (2.2 μm) were visible even though EX Hya was two magnitudes brighter than it is at quiescence.

We have observed this system in quiescence with both ISAAC at the VLT, and with NIRSPEC (McLean et al. 1998) at the Keck Observatory. Both of these spectra are presented in Fig. 3, where we compare them to the spectra of two M dwarfs. In both datasets, the secondary star was prominent. The strength of the Ca I triplet in this system

indicates an earlier spectral type than either of our first two objects, best matching an M5 dwarf. In contrast to its longer period IP cousins, GK Per and AE Aqr (see Harrison et al. 2007), EX Hya has CO absorption features that appear to be relatively normal. EX Hya has a high precision *HST* parallax (Beuermann et al. 2003) that gives a distance of 64.5 ± 1.2 pc. At this distance, if we assign a value of M_K appropriate for an M5 V dwarf, the secondary would supply 44% of the observed *K*-band flux.

3.4. VW Hyi

VW Hyi ($P_{\text{orb}} = 1.78$ hr) is an SU UMa type CV, with outbursts roughly every 28 days and super-outbursts approximately every 183 days. Mennickent et al. (2004) examined this system with ISAAC at low resolution, finding evidence for an $L0 \pm 2$ dwarf based on fitting of the *J*-band with a power-law disk component and a stellar template. Smith et al. (2006) estimate a primary mass of $M_1 = 0.71_{-0.26}^{+0.18} M_{\odot}$ from the gravitational redshift of the Mg II $\lambda 4481$ absorption line on the white dwarf. A mass ratio of $q = M_2/M_1 = 0.148 \pm 0.004$ from the superhump-period excess (Patterson 1998) implies a secondary mass of $M_2 = 0.11 \pm 0.03 M_{\odot}$. Knigge (2006) predicts an M5 dwarf donor at this orbital period. VW Hyi is one of the brightest of the (non-magnetic) sub-gap CVs, having $K_{2\text{MASS}} = 11.70$.

Our ISAAC spectrum of VW Hyi is shown in Fig. 3. The strength of the Na I doublet relative to that of the Ca I triplet point to a mid-M spectral type, and we find good agreement with an M4 dwarf. At this spectral type, the CO features are close to their expected strength. Longward of the first prominent CO bandhead around $2.29 \mu m$ the spectrum becomes very noisy, and the spike at the red end of the spectrum is due to low S/N, not CO disk emission filling of the bandheads (see Howell et al. 2010, Fig. 11). Strangely, the spectral region between 2.21 and $2.26 \mu m$ has a number of absorption features, which we tentatively associate with Fe I, that are much more consistent with a

very late M-type dwarf (M9V). While the S/N of this spectrum is not particularly high, each of these features has the correct depth and width (as some are doublets), matching the features in the M9V. Later types, however, do not match the strengths of the other prominent spectral features, and we find that the overall spectrum is clearly inconsistent with an L0 dwarf.

3.5. Z Cha

Z Cha ($P_{orb} = 1.79$ hr) is an SU UMa type CV, with recurrence times of ~ 17 days and ~ 287 days for normal and superoutbursts respectively and $K_{2MASS} = 13.31$. Wade & Horne (1988) observed Z Cha spectroscopically, obtaining a radial velocity curve of the secondary star using the Na I doublet at $\lambda 8183$ and $\lambda 8194$. Combining that with a mass ratio of the system derived from eclipses by Wood et al. (1986), they calculate system parameters of $M_1 = 0.84 \pm 0.09 M_{\odot}$ and $M_2 = 0.125 \pm 0.014 M_{\odot}$. Wade & Horne (1988) also find evidence for an M5.5 secondary star, based on TiO band strengths. Since the orbital period for Z Cha is so similar to VW Hyi, we would expect to find an M5 dwarf donor.

The spectrum of Z Cha using ISAAC is shown in Fig. 4. It must be noted that the blue portion of the spectrum was observed some 4 months *after* the redward side, as shown in Table 1. The AAVSO archive has magnitude estimates during both time periods, showing that the system was in between outbursts at the epochs of the VLT observations, with similar visual magnitudes. The spectrum is heavily contaminated by the accretion disk, making proper identification of the spectral type of the secondary star highly uncertain. If we accept the M5 classification, then the CO features are much weaker than they should be. This spectral type is consistent with the observed strength of both the Ca I triplet and the Na I doublet.

3.6. V893 Sco

V893 Sco ($P_{\text{orb}} = 1.82$ hr) is an eclipsing SU UMa system with $K_{2\text{MASS}} = 12.68$. Mason et al. (2001) obtained optical spectroscopy from which they derived an $H\alpha$ radial velocity curve consistent with $M_1 = 0.89 M_{\odot}$ and $q = M_2/M_1 = 0.19$, giving a secondary mass of $M_2 = 0.17 M_{\odot}$. We again expect an M5 dwarf donor at this orbital period, as we did for both VW Hya and Z Cha. Thorstensen (2003) was able to measure the parallax of this system, putting the distance at 155^{+55}_{-34} pc. The Na I doublet and the first overtone of CO are visible in our spectrum of V893 Sco, but the quality of these data are low, and the Ca I triplet remains undetected. This spectrum does show a water vapor break, and this is indicative of a later type secondary than seen in Z Cha, and we suggest that the spectral type is $> M6$. An M6V at the distance of V893 Sco would have $K = 15.21$. Given that the secondary star is visible in the K -band suggests that V893 Sco is closer than given by the lower limit of the measured parallax.

3.7. RZ Leo

RZ Leo ($P_{\text{orb}} = 1.83$ hr) is a member of the small family of WZ Sge-like CVs, sometimes called “TOADs” (Howell et al. 1995), that exhibit infrequent, but very large (≥ 6 mag) SU UMa-type outbursts. Patterson et al. (2003) reports both an orbital and superhump period from spectroscopy and long term photometry of 1.82492 and 1.888 hours, respectively. Knigge (2006) estimates, assuming a primary mass of $M_1 = 0.75 M_{\odot}$, an M5V secondary with a mass of $M_2 = 0.114 M_{\odot}$ and a radius of $R_2 = 0.171 R_{\odot}$. This spectrum was recently presented by Howell et al. (2010), and is included here for completeness.

The K -band spectrum of RZ Leo from NIRSPEC at Keck as described in §2.2 is shown in Figure 5. RZ Leo is the faintest of the objects in our survey (by two magnitudes),

having $K_{2\text{MASS}} = 15.39$. Unlike the prototype TOAD WZ Sge, whose secondary has proved elusive, the donor star in RZ Leo is easily seen. It appears to be an $M4\pm 1$ with normal CO features, based on the strengths of the Na I doublet and the Ca I triplet. This spectral type is similar to the M5 assigned by Mennickent & Diaz (2002) from SED fitting of lower resolution ISAAC J , H , and K -band spectra.

3.8. WX Hyi and TY PsA

WX Hyi ($P_{\text{orb}} = 1.80$ hr) is an SU UMa type CV, and was first spectroscopically examined by Schoembs & Vogt (1981). Using optical spectroscopy, they found a primary mass of $M_1 = 0.9 \pm 0.3 M_{\odot}$ and mass ratio $q = M_2/M_1 = 1.8$ based on a radial velocity study. Ritter & Kolb used these to estimate a secondary mass of $M_2 = 0.16 \pm 0.05 M_{\odot}$. We have been unable to find any other information about the possible spectral type of the secondary star. Even though it is relatively bright, $K_{2\text{MASS}} = 12.96$, no identifiable absorption features can be seen in its infrared spectrum (see Fig. 1). In fact, in contrast to every other object, it shows a slightly rising continuum at the red end of the K -band.

TY PsA ($P_{\text{orb}} = 2.02$ hr) is a rarely studied SU UMa type CV. Prior spectroscopic examinations of this system (Warner et al. 1989; O’Donoghue & Soltynski 1992) found no radial velocity variations, suspecting that this system has an extreme mass ratio and therefore a sub-stellar companion. Mennickent et al. (2004) examined this system in the infrared with ISAAC previously, and found no features of the secondary star. At this slightly longer orbital period, Knigge (2006) predicts an M4.5 dwarf donor. Unlike WX Hyi, the continuum for TY PsA shows a slight decline at the red end of its spectrum. Given the considerable contamination needed to wash-out the other absorption features, this would suggest a late spectral type ($> M6$) so as to have a large enough water vapor feature to affect the continuum. Given that it has an almost identical brightness to V2051

Oph ($K_{2\text{MASS}} = 13.58$ vs. 13.53), and we used the same exposure time as on that object, the 2MASS survey must have caught this object somewhat brighter than it is at true quiescence. Using our raw data shows that the count rate for TY PsA was only half that of V2051 Oph, suggesting that at the time of observation $K \approx 14.3$.

4. Discussion

We have conducted a moderate resolution spectroscopic survey of nine CVs below the period gap. We clearly detect features from the secondary stars in six of these objects, and place constraints on two systems based on suspected water vapor declines seen in their continua. All of the secondary stars appear to be mid- to late-type M dwarfs and are consistent with the measured/estimated masses available in the literature. Our results are summarized in Table 3. In Figure 6 we have plotted our new spectral type estimates on the empirical donor sequence (Knigge 2006). We have also added the results from Harrison et al. (2009) for EI Psc and VY Aqr to this diagram for completeness. Overall we find that our estimates fit well with Knigge’s empirical fit.

With the results of this diagram in hand, Knigge (2006) discussed how to use it to provide lower limits on the distance using single epoch K -band measurements, with the warning that the distance is on average underestimated by a factor of 1.75. By combining our spectroscopically determined spectral types with the observed infrared photometry, we find that this procedure can only provide a weak constraint on the distances to sub-gap CVs. In Figure 7 we plot the 2MASS colors for our program objects, along with the main sequence color-color relationship. Two objects fall near the main sequence relationship: EI Psc, and RZ Leo. As discussed in Harrison et al. (2009) EI Psc ($P_{\text{orb}} = 1.07$ hr) acts just like a main sequence K5 dwarf in the infrared, and apparently suffers from very little accretion disk contamination. The other object, RZ Leo, has such uncertain photometry

($\sim \pm 0.2$ mags, see Table 2) that its position in the diagram is very poorly constrained and does not allow for any conclusions. The objects with the best-determined spectral types in our survey are V2051 Oph, V436 Cen, VW Hya, and EX Hya. The first three of these objects have very similar colors (especially in $H - K$), but range from M8 (V436 Cen) to M4 (VW Hya). This result suggests that there is substantial disk contamination occurring in both V2051 Oph and V436 Cen — yet these two objects have secondary stars that are just as easily seen as those in VW Hya and EX Hya. It must also be noted that all of these objects are capable of showing quiescent variability on the order of $\Delta V = 0.1 - 0.3$ mag.

To underscore the problems associated with estimating parameters from IR colors alone, we consider the two systems in our survey with measured parallaxes: EX Hya, and V893 Sco. Using the Knigge relationship for EX Hya, one derives a lower limit to its distance of $d = 30$ pc, while the parallax gives 62 pc. The relationship would predict a distance of 53 pc for V893 Sco versus the parallax measurement of 155 pc. Both of these limits are less than one half of what is measured, even accounting for the significant uncertainty in the parallax for V893 Sco.

We show this further by assembling all of the published parallaxes for CVs (but excluding polars, and AM CVn systems) and derive an $M_K - P_{\text{orb}}$ relationship (parallaxes from Harrison et al. 2004a; Thorstensen 2003; Thorstensen et al. 2008), presented as Fig. 8. While there is clearly a lower limit on M_K that depends on P_{orb} , *at any one orbital period the spread in M_K is two magnitudes or more*. Deconvolving the infrared colors of CVs remains a difficult task, and infrared photometry should be used with caution when estimating *any* intrinsic parameter of these systems.

4.1. Examination of CO Strength Across All CV Subtypes

Table 4 summarizes all the relevant observations at a high enough resolution in the K -band to directly measure absorption lines from the secondary star in all CV subtypes completed thus far. Most of the data in Table 4 have been compiled from Howell et al. (2010), and we have included those data here after checking on the original references for each system. While we are dealing with a small sample size, a few general trends are clear: pre-CVs, sub-gap systems, and highly magnetic polars generally show normal CO band strengths. Eighteen of the nineteen pre-CV systems observed show CO appropriate for their spectral type, with the exception of the triple system HS1136 which showed no absorption features from the secondary star, likely due to the presence of an extremely hot WD in the system. Among the magnetic CV’s, only three of the eleven show unusual CO strengths: GK Per, AE Aqr, and V1309 Ori. Both AE Aqr and GK Per are thought to harbor subgiant secondary stars (Harrison et al. 2005a; Howell et al. 2010), so this is not unexpected. Among the non-magnetic, long period systems, there are thirteen out of nineteen systems that either show absent or weakened CO features, and five systems that appear more or less normal. Including the systems presented here, three out of the twelve short period sub-gap systems clearly show weaker CO than expected for their spectral type: Z Cha, VY Aqr, and EI Psc. There is strong evidence for a hot K-type secondary in EI Psc (Thorstensen et al. 2002), unexpected given its ultra-short period ($P_{\text{orb}} = 1.07$ hr). It should have a very late type companion, but the IR spectroscopy confirms the mid-K spectral type, and reveals a secondary star with extraordinarily weak CO features. The results for VY Aqr ($P_{\text{orb}} = 1.51$ hr) are not as clear, as the spectral type of the secondary star derived from the VLT ($\sim M6$) and Keck ($\sim M0$) datasets are quite different. No matter the classification, the CO features in the secondary star of VY Aqr were extremely weak. For Z Cha, the case is not as strong, though it appears that the CO strength is weaker than would be expected. Further observations are needed to verify the spectral type of the donor

star in Z Cha.

In all the cases where we see weak or non-existent CO absorption in the atmosphere of the secondary star, we interpret this as a deficit in the C abundance. While we have IR spectra for a small percent of all CVs, UV spectroscopy is uncovering evidence of C depleted material through the detection of unusual N V/C IV line ratios. Studies in the UV (e.g., Bonnet-Bidaud & Mouchet 1987; Szkody & Silber 1996; Mauche et al. 1997) have long shown that the N V/C IV ratio in the UV spectra of a number of cataclysmic variables was very high, suggesting a strong enhancement of nitrogen and/or a deficit of carbon in the accretion disk or in the WD photosphere. UV observations of a large sample of polars by Araujo-Betancor et al. (2005), however showed that they had normal N V/C IV line ratios. These two taken together imply that matter transferred from the secondary star in non-magnetic systems is the source of the UV abundance anomalies, and that these stars have CNO processed material in their atmospheres.

Table 4 highlights the five cases where we do have deficiencies in C seen both in the UV and in the IR: EY Cyg, EI Psc, AE Aqr, U Gem, and V1309 Ori. The most natural explanation of this result is that C depleted material is being transferred from the secondary star to the white dwarf/accretion disk. Howell et al. (2010) provide a discussion of why the C deficient material must be flowing from the secondary star onto the white dwarf/accretion disk and not in the other direction.

The link between the abundances seen in the UV and the IR can be further strengthened by looking at two cases where normal C abundances in the UV are matched by normal C abundances in the IR: SS Aur and VW Hyi. SS Aur is a typical dwarf nova above the period gap ($P_{\text{orb}} = 4.26$ hr), and appears to have normal CO features in the spectrum presented by Howell et al. (2010). Analysis of the UV spectra of SS Aur by Godon et al. (2008) show that it has normal C and N abundances. Our spectrum of VW Hyi presented here show

it to be a normal M4 dwarf, and while previous UV spectroscopy suggested a sub-solar C abundances (Sion et al. 1996), more recent analysis (E. Sion, private communication) suggests that the C abundance in VW Hyi is close to solar. To put this potential UV-IR CNO connection to the test, it should be seen whether an anomaly in one can be used to predict an anomaly in the other. It is therefore critical to obtain IR spectra of the three sub-gap systems that are known to show unusual UV C/N ratios: BC UMa, SW UMa, and BW Scl (Gänsicke et al. 2005).

It is a challenge to completely explain why pre-CV, short period, and magnetic systems in general appear to have normal C abundances, while the long period systems do not. One possible way to explain “normal” C abundances at short periods was demonstrated by Marks & Sarna (1998). For their models where the secondary has evolved off of the main sequence before contact, they show that the surface C abundance in the secondary star declines throughout most of its life as a CV (see their Fig. 16) until its mass reaches $\sim 0.3 M_{\odot}$. After this point the surface C abundance returns to normal as material from deeper layers within the star, unaffected by the CNO cycle that operated prior to contact, are convected to the surface. However, the standard model for CV evolution does not give the secondary star sufficient time to evolve off the main before starting mass transfer. Still, if the angular momentum braking mechanisms are less efficient than is currently believed, then the secondary would have additional time to undergo nuclear evolution.

To explore this possibility, we briefly consider the standard paradigm for the formation of the period gap. As the secondary approaches the fully convective boundary at the top of the period gap ($P_{\text{orb}} \approx 3$ hrs, $M_2 \approx 0.2 - 0.3 M_{\odot}$), magnetic braking is believed to be disrupted as the tachocline, the interface region of strong shear between the radiative and convective zones (and believed to be the site responsible for generating the magnetic field) is lost, shutting down the dynamo (see Browning et al. 2010, and references therein).

Currently, however, there exists evidence both for, and against, the disruption in magnetic braking near the convective boundary.

Schreiber et al. (2010) found evidence for this disrupted magnetic braking mechanism in a survey of SDSS post common envelope binaries (PCEBs), examining the fraction of PCEBs compared to non-interacting white dwarf plus main sequence binaries (WDMS). In the case of disrupted magnetic braking, there is a predicted steep decrease in the number of PCEBs at the fully convective boundary due to their much longer evolutionary timescales. This was seen in their survey of SDSS selected systems. Also supporting the disrupted magnetic braking scenario, Browning et al. (2010) was only able to detect rotation ($v \sin i \geq 2.5 \text{ km s}^{-1}$) in seven out of 122 M dwarfs, of which four of these were past the fully convective boundary. They suggest that this demonstrates that magnetic braking is less effective at the convective boundary. It is interesting to note, however, that the seven stars with detected rotation all showed high levels of stellar activity.

Conversely, Andronov & Pinsonneault (2004) state that there is nothing “magical” about the angular momentum loss rate or stellar activity levels at the fully convective boundary. This is supported by additional data for low mass stars in clusters (c.f. Scholz et al. 2009, and references therein). In fact, Donati et al. (2008) show that there is a dramatic *increase* in the dynamo generating processes at the fully convective boundary

Supposing that the secondary star becoming fully convective is not a reasonable method for producing the period gap, is there an alternative method for shutting down the magnetic braking? One possible method to offset the influence of the high levels of magnetic activity seen at the fully convective boundary, with the weaker magnetic braking observed for these stars, is to suppose that the field topology changes from a predominantly large scale toroidal configuration seen in stars with radiative zones (see Solanki 2009), to a much more complex, non-axisymmetric topology in fully convective stars. In this case, the global

field might more closely resemble a collection of multi-polar structures whose individual field strengths fall off rapidly with distance, resulting in a much weaker global field than in the dipole case. Such fields would have limited numbers of “open field” lines along which to transport material, and thus much lower magnetic braking (see Collier Cameron 2002). But recent observations by Donati et al. (2006) show that V374 Peg, a rapidly rotating ($P_{\text{rot}} = 10.69$ hr), fully convective M4V has a large scale axisymmetric poloidal (dipole-like) field. A similar result was found for the M4 dwarf GL 490B by Phan-Bao et al. (2009). Recent polarimetric observations across the M dwarf sequence (Donati et al. 2008; Morin et al. 2008, 2010) point towards a sharp transition in magnetic field topology at $0.5 M_{\odot}$, below which the poloidal field topology dominates and its strength increases as mass decreases. Morin et al. (2010) do note that it is possible to see wildly different magnetic topologies between objects with similar stellar parameters, suggesting that another parameter (perhaps age?) could play a role in the observed topology. In any case, there is strong evidence that the majority (85%) of the magnetic energy remains locked-away in smaller structures (Reiners & Basri 2009; Morin et al. 2008). Perhaps it is the factor of ~ 3 increase (compared to V374 Peg) in rotational velocity for CV secondaries at the top of the period gap that is sufficient to eliminate the large scale poloidal field and disrupt the otherwise efficient magnetic braking.

One characteristic of rapid rotating late-type stars is that much of the stellar activity is located closer to the poles of these objects (see Bushby 2003, and references therein). In some CVs polar spots are seen (Watson et al. 2006), while in others the spots are more equatorial (Watson et al. 2007). Cohen et al. (2009) show that if a spot is located near the pole, the stellar wind structure is dramatically affected, and that total mass and angular momentum loss is substantially higher than if the spots were equatorial. Unless it is found that the spots on CVs are preferentially located near the equatorial regions, this explanation seems unable to produce the desired result.

While observations of the magnetic field structures in low mass stars is improving, as is our understanding of the generation of their magnetic dynamos, the extension of this knowledge to explain the CV period gap is incomplete. Since there is one, and only one property that all CVs at the top of the period gap must share, a three hour rotation period, it must be that rotation somehow quenches the efficient magnetic dynamo generation in fully convective stars.

5. Conclusions

We have performed a near-IR spectroscopic moderate resolution survey of nine sub-gap CVs, detecting a signature of the secondary star in eight systems. We demonstrate an important link between abundance anomalies seen in the UV and in the IR, as well as the reverse cases where the lack of abundance anomalies appear. Our clear detections show that future phase-resolved spectroscopy will further constrain the nature of these secondary stars by obtaining radial velocity measurements and therefore masses of the secondary stars in these systems.

While our results indicated a large fraction of sub-gap CVs contain a normal CO abundance, we have insufficient objects to fully test this idea at present. Ongoing analysis and modeling of these data presented here will allow us to explore the CO bands seen in our spectra. To fully assess the $^{12}\text{C}/^{13}\text{C}$ ratio which gives the best indication and possibility to see if the secondary star contains any CNO processed material (Dhillon et al. 2002), but will require higher quality data.

We thank the anonymous referee for their useful and helpful comments.

This work is based on observations made with ESO Telescopes at the Cerro Paranal Observatory under program ID 081.D-0225.

Some of the data presented herein were obtained at the W.M. Keck Observatory, which is operated as a scientific partnership among the California Institute of Technology, the University of California and the National Aeronautics and Space Administration. The Observatory was made possible by the generous financial support of the W.M. Keck Foundation. The authors wish to recognize and acknowledge the very significant cultural role and reverence that the summit of Mauna Kea has always had within the indigenous Hawaiian community. We are most fortunate to have the opportunity to conduct observations from this mountain.

This publication makes use of data products from the Two Micron All Sky Survey, which is a joint project of the University of Massachusetts and the Infrared Processing and Analysis Center/California Institute of Technology, funded by the National Aeronautics and Space Administration and the National Science Foundation.

RH would like to thank the New Mexico Space Grant consortium for Graduate Research Fellowship support from 2007-09.

Facilities: VLT:Antu (ISAAC), Keck:II (NIRSPEC)

REFERENCES

- Andronov, N., & Pinsonneault, M. H. 2004, *ApJ*, 614, 326
- Araujo-Betancor, S., Gänsicke, B. T., Long, K. S., Beuermann, K., de Martino, D., Sion, E. M., & Szkody, P. 2005, *ApJ*, 622, 589
- Baptista, R. et al. 1998, *MNRAS*, 300, 233
- Beuermann, K. & Reinsch, K 2008, *A&A*, 480, 199
- Beuermann, K., Harrison, T. E., McArthur, B. E., Benedict, G. F., Gänsicke, B. T. 2003, *A&A*, 412, 821
- Bonnet-Bidaud, J. M., & Mouchet, M. 1987, *A&A*, 188, 89
- Bushby, P. J. 2003, *MNRAS*, 342, L15
- Browning, M. K., Basri, G., Marcy, G. W., West, A. A., & Zhang, J. 2010, *AJ*, 139, 504
- Cohen, O., Drake, J. J., Kashyap, V. L., & Gombosi, T. I. 2009, *ApJ*, 699, 1501
- Collier Cameron, A. 2002, *The Physics of Cataclysmic Variables and Related Objects*, 261, 11
- Cushing W. D. et al. 2005, *ApJ*, 623, 1115
- Dhillon, V.S., & Marsh, T.R. 1995, *MNRAS*, 275, 89
- Dhillon, V.S., Littlefair, S.P., Howell, S.B., Ciardi, D.R., Harrop-Allin, M.K., & Marsh, T.R. 2000, *MNRAS*, 314, 826
- Dhillon, V. S., Littlefair, S. P., Marsh, T. R., Sarna, M. J., & Boakes, E. H. 2002, *A&A*, 393, 611

Donati, J.-F., Forveille, T., Cameron, A. C., Barnes, J. R., Delfosse, X., Jardine, M. M., & Valenti, J. A. 2006, *Science*, 311, 633

Donati, J.-F., et al. 2008, *MNRAS*, 390, 545

Gänsicke, B. T., et al. 2003, *ApJ*, 594, 443

Gänsicke, B. T., Szkody, P., Howell, S. B., & Sion, E. M. 2005, *ApJ*, 629, 451

Godon, P., Sion, E. M., Barrett, P. E., Hubeny, I., Linnell, A. P., & Szkody, P. 2008, *ApJ*, 679, 1447

Harrison, T. E., Johnson, J. J., McArthur, B. E., Benedict, G. F., Szkody, P., Howell, S. B., & Gelino, D. M. 2004a, *AJ*, 127, 460

Harrison, T.E., Osborne, H.L. & Howell, S.B. 2004b, *AJ*, 127, 3493

Harrison, T. E. et al. 2005a, *ApJ*, 632, 123

Harrison, T.E., Osborne, H.L. & Howell, S.B. 2005b, *AJ*, 129, 2400

Harrison, T. E., Campbell, R. K., Howell, S. B., Cordova, F. A., & Schwope, A. D. 2007, *ApJ*, 656, 444

Harrison, T.E., Bornak, J., Howell, S.B., Mason, E., Szkody, P., & McGurk, R. 2009, *AJ*, 137, 4061

Harrison, T. E., Bornak, J., Rupen, M. P., & Howell, S. B. 2010, *ApJ*, 710, 325

Harrison, T.E. 2010, Private Communication

Howell, S. B., Szkody, P. & Cannizzo, J. K. 1995, *ApJ*, 439, 337

Howell, S.B., Nelson, L.A. & Rappaport, S. 2001, *ApJ*, 550, 897

- Howell, S.B., Harrison, T.E., & Szkody, P. 2004, *ApJ*, 602, L49
- Howell, S. B. 2005, *The Astrophysics of Cataclysmic Variables and Related Objects*, 330, 67
- Howell, S. B., Walter, F. M., Harrison, T. E., Huber, M. E., Becker, R. H., & White, R. L. 2006, *ApJ*, 652, 709
- Howell, S. B., Harrison, T. E., Szkody, P., & Silvestri, N. M. 2010, *AJ*, 139, 1771
- Ishioka, R., Sekiguchi, K., & Maehara, H. 2007, *PASJ*, 59, 929
- Ivanov, V. D., Rieke, M. J., Engelbracht, C. W., Alonso-Herrero, A., Rieke, G. H., & Luhman, K. L. 2004, *ApJS*, 151, 387
- Jameson, R. F., King, A. R., & Sherrington, M. R. 1980, *MNRAS*, 191, 559
- Knigge, C. 2006, *MNRAS*, 373, 484
- Long, K. S., & Gilliland, R. L. 1999, *ApJ*, 511, 916
- Marks, P. B., & Sarna, M. J. 1998, *MNRAS*, 301, 699
- Mason, E., Skidmore, W., Howell, S. B., & Mennickent, R. E. 2001, *ApJ*, 563, 351
- Mauche, C. W., Lee, Y. P., & Kallman, T. R. 1997, *ApJ*, 477, 832
- Mauche, C. W. et al. 2009, *IBVS*, 5876, 1
- McLean, I. S. et al. 1998, *Proc. SPIE*, 3354, 566
- Mennickent, R. E., & Diaz, M. P. 2002, *MNRAS*, 336, 767
- Mennickent, R. E., Diaz, M. P. & Tappert, C. 2004, *MNRAS*, 347, 1180
- Moorwood, A. et al. 1998, *The Messenger*, 94, 7

- Morin, J., et al. 2008, MNRAS, 390, 567
- Morin, J., Donati, J.-F., Petit, P., Delfosse, X., Forveille, T., & Jardine, M. M. 2010, MNRAS, 1077
- North, R. C., Marsh, T. R., Moran, C. K. J., Kolb, U., Smith, R. C., & Stehle, R. 2000, MNRAS, 313, 383
- O’Donoghue, D., & Soltynski, M. G. 1992, MNRAS, 254, 9
- Patterson J. 1998, PASP, 110, 1132
- Patterson, J. 2001, PASP, 113, 736
- Patterson, J. et al. 2003, PASP, 115, 1308
- Phan-Bao, N., Lim, J., Donati, J.-F., Johns-Krull, C. M., & Martín, E. L. 2009, ApJ, 704, 1721
- Reiners, A., & Basri, G. 2009, A&A, 496, 787
- Ritter H. & Kolb U. 2003, A&A, 404, 301 (update RKcat7.12, 2009)
- Schmidt, G. D., & Stockman, H. S. 2001, ApJ, 548, 410
- Schoembs, R., & Vogt, N. 1981, A&A, 97, 185
- Scholz, A., Eislöffel, J., & Mundt, R. 2009, MNRAS, 400, 1548
- Schreiber, M. R., et al. 2010, A&A, 513, L7
- Sion, E.M., Cheng, F.-H., Huang, M., Hubeny, I., & Szkody, P. 1996, ApJ, 471, L41
- Sion, E. M., Winter, L., Urban, J. A., Tovmassian, G. H., Zharikov, S., Gänsicke, B. T., & Orío, M. 2004, AJ, 128, 1795

- Skrutskie, M. F., et al. 2006, *AJ*, 131, 1163
- Smith, A. J., Haswell, C. A. & Hynes, R. I. 2006, *MNRAS*, 369, 1537
- Solanki, S. K. 2009, *Astronomical Society of the Pacific Conference Series*, 405, 135
- Szkody, P., & Silber, A. 1996, *AJ*, 112, 289
- Tappert, C., Gänsicke, B.T., Schmidtbreick, L., Mennickent, R.E., & Navarrete, F.P. 2007, *A&A*, 475, 575
- Thorstensen, J. R., Fenton, W. H., Patterson, J. O., Kemp, J., Krajci, T., & Baraffe, I. 2002, *ApJ*, 567, L49
- Thorstensen, J. R. 2003, *AJ*, 126, 3017
- Thorstensen, J. R., Lépine, S., & Shara, M. 2008, *AJ*, 136, 2107
- Wade, R. A. & Horne, K. 1988, *ApJ*, 324, 411
- Warner, B., O'Donoghue, D., & Wargau, W. 1989, *MNRAS*, 238, 73
- Watson, C. A., Dhillon, V. S., & Shahbaz, T. 2006, *MNRAS*, 368, 637
- Watson, C. A., Steeghs, D., Dhillon, V. S., & Shahbaz, T. 2007, *Astronomische Nachrichten*, 328, 813
- Wood, J. et al. 1986, *MNRAS*, 219, 629

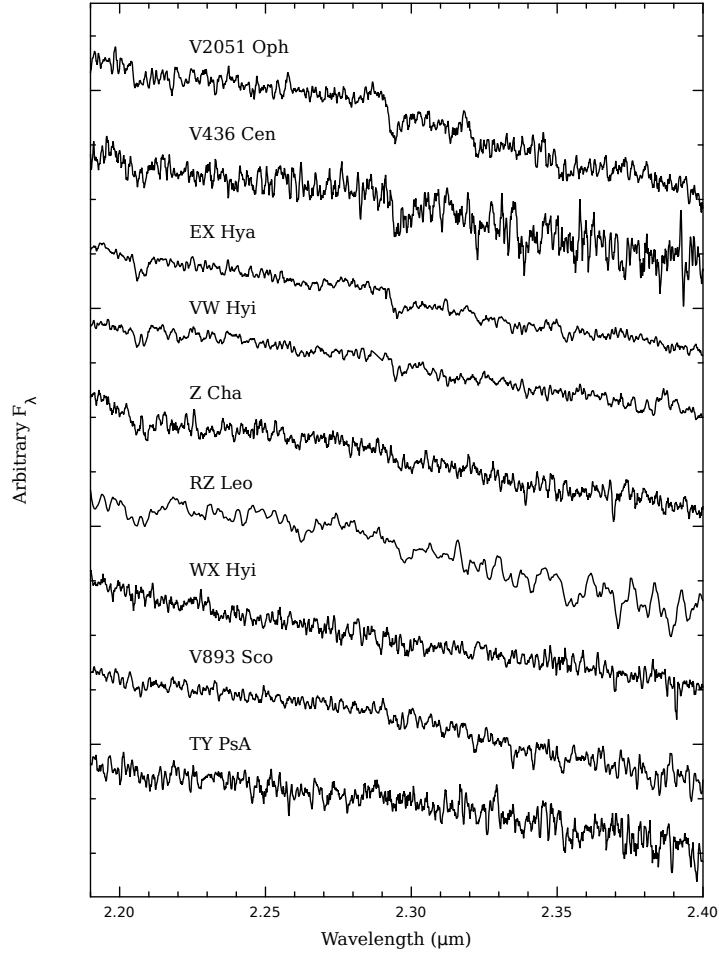


Fig. 1.— The VLT spectra of our program objects, except that for RZ Leo which was obtained using NIRSPEC on Keck II.

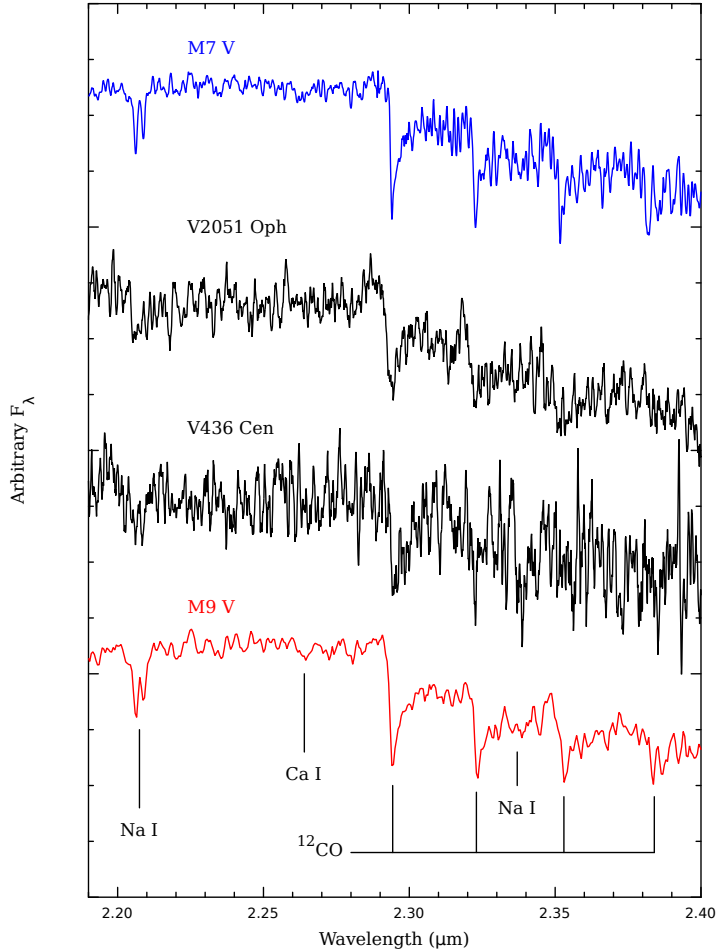


Fig. 2.— The spectra of V2051 Oph and V436 Cen compared to the spectra of two late-type templates an M7V (LHS 3003), and an M9V (LHS 2065, from the IRTF Spectral Library). The strongest absorption features, as used for spectral type determination, are indicated. The object spectra presented here have been vertically stretched for presentation purposes to more clearly demonstrate their similarity to the spectral type classification derived from the continuum subtracted data as described in the text. The lack of Ca I absorption, and the fact that the first overtone absorption of CO is stronger than the Na I doublet, indicate a very late spectral type. We estimate spectral types of M7 for V2051 and M8 for V436 Cen.

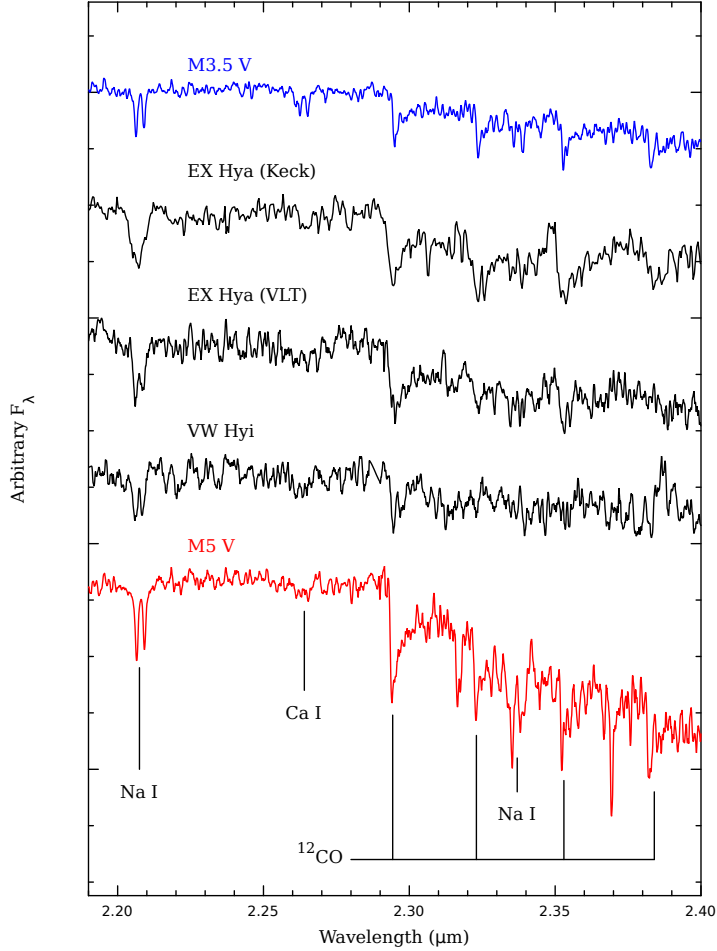


Fig. 3.— The spectra of the intermediate polar EX Hya, and the SU UMa system VW Hyi, compared to the spectra of two mid-M dwarfs (the M3.5V is LHS 427, and the M5V template is LHS 2347). EX Hya was observed with both Keck (upper spectrum) and with the VLT (lower spectrum). As in Fig. 2, the object spectra have been stretched for presentation purposes. The relative strengths of Ca I triplets indicate spectral types near M5 for EX Hya, and M4 for VW Hyi.

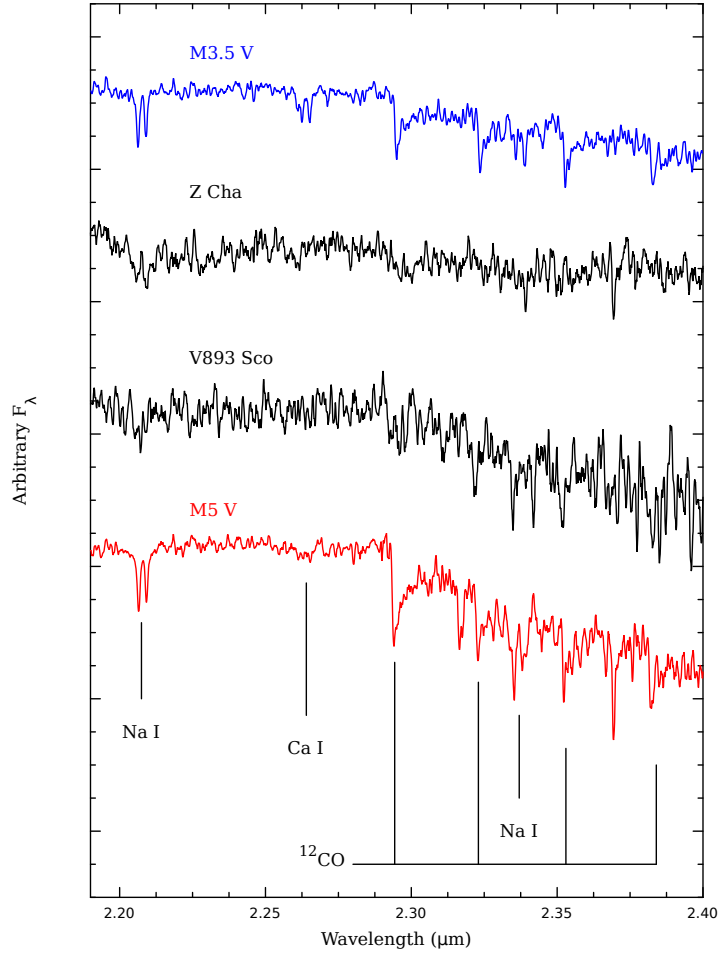


Fig. 4.— The spectra of Z Cha and V893 Sco compared to two mid-M type templates. In Z Cha, the Na I doublet is clearly seen, as well as a hint of the Ca I triplet, suggesting a mid-M type secondary star. The CO features, however, are quite weak, suggesting a C deficit. The spectrum for V893 Sco is poorer, barely showing the Na I doublet, but it clearly has CO absorption, indicating that it has a slightly later spectral type than Z Cha.

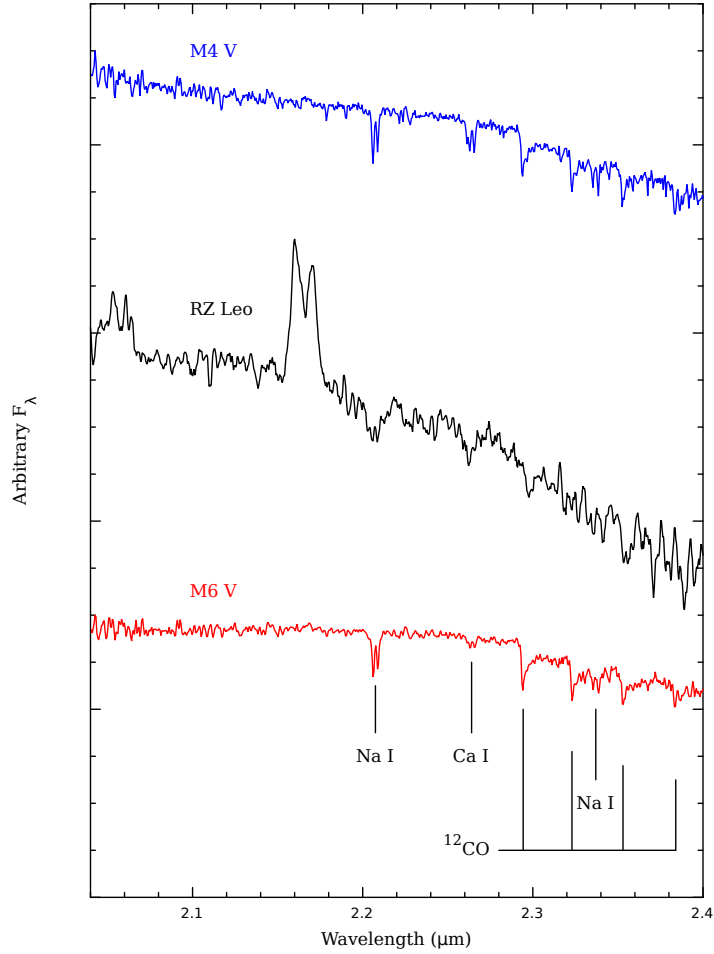


Fig. 5.— The NIRSPEC spectrum of RZ Leo compared to two mid-M type dwarfs (both from the IRTF Spectra library). The NIRSPEC data cover a larger range in wavelength (at lower spectral resolution) than the ISAAC spectra. The two strong emission lines are due to H I Br γ (at 2.16 μm) and He I (at 2.06 μm). The (unstretched) spectrum of RZ Leo clearly shows a strong decline due to water vapor.

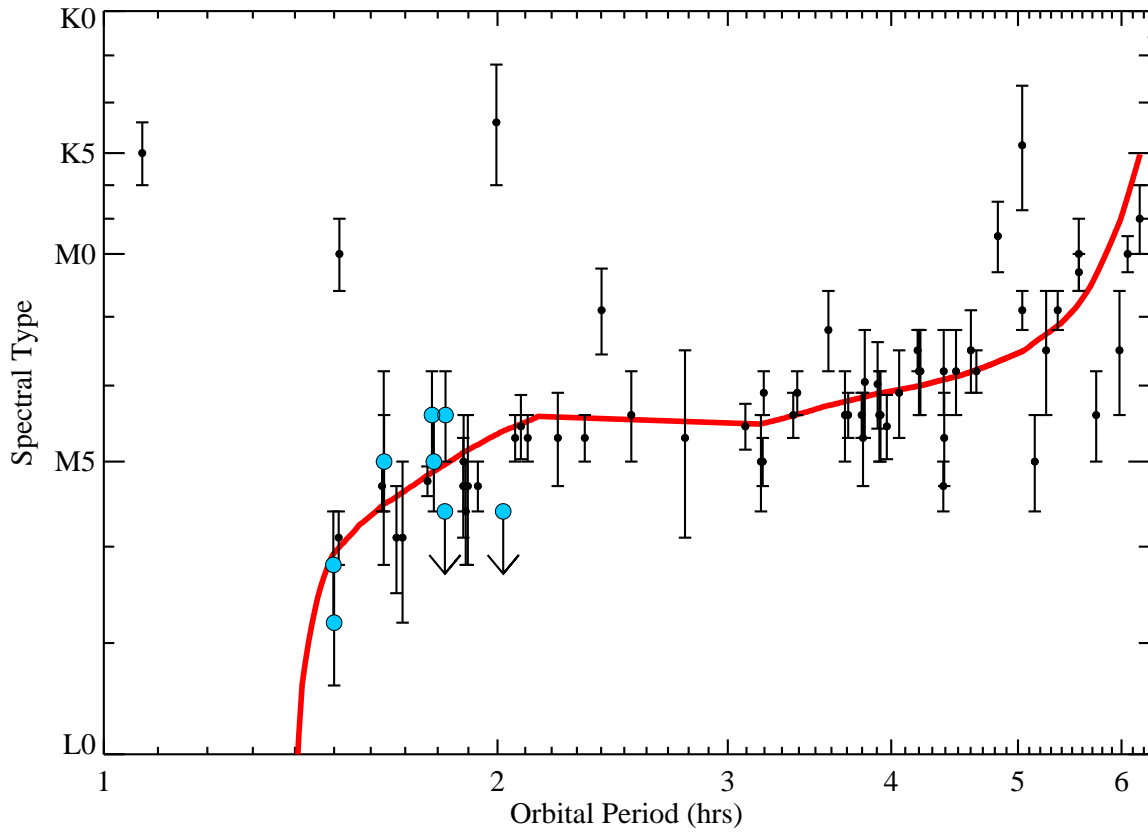


Fig. 6.— The Spectral type vs. P_{orb} relationship from Knigge (2006) with the additional results from the analysis of the VLT ISAAC spectroscopy plotted as larger circles (blue in the online version).

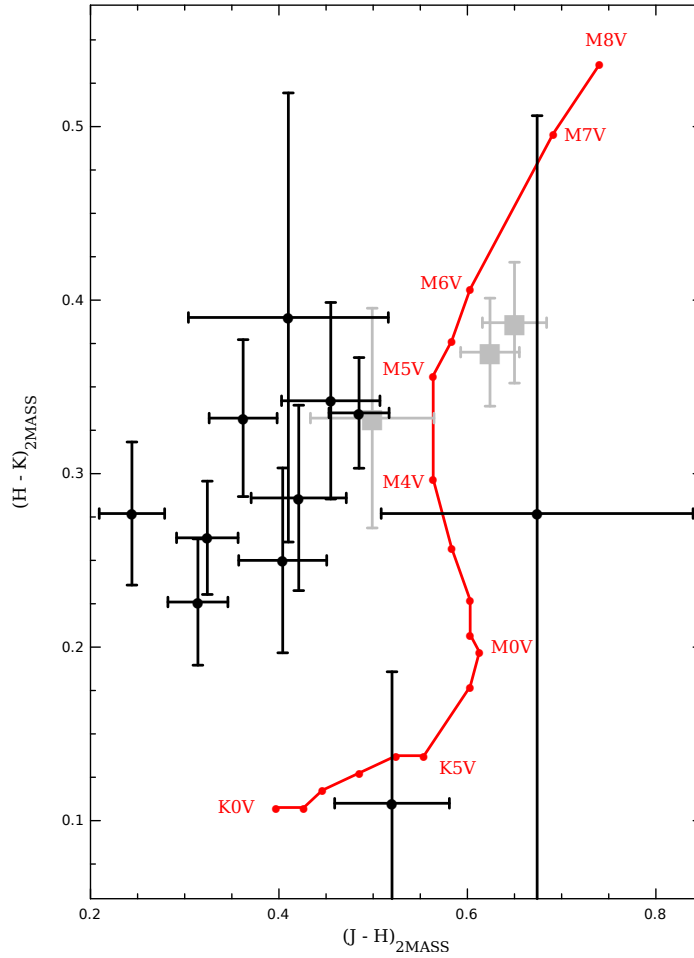


Fig. 7.— The infrared color-color plot for the program objects generated using the 2MASS data base. In addition, we have added two additional sub-gap CVs with detected secondaries, EI Psc and VY Aqr, using data from Harrison et al. (2009). Also shown is the main sequence color-color relationship (labeled line) from K0V to M8V, and the reference M stars (see §2.4) observed in our sample (grey boxes).

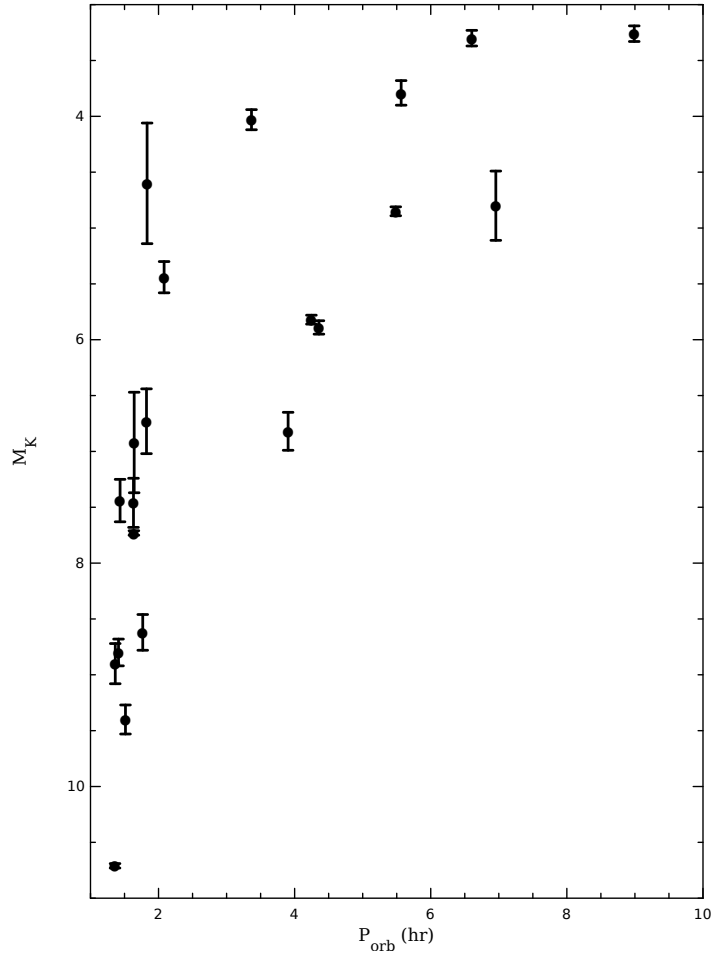


Fig. 8.— The M_K vs. P_{orb} relationship for cataclysmic variables with measured parallaxes (excluding “polars” and AM CVn systems).

Table 1. Observation Log

System	Observation Date (UT)	Observation Time (Midpoint, UT)	Exp Time (s)	# Exp	Integration Time (s)	Phase Covered (%)
V2051 Oph	2008-05-12	07:51:30	70.0	30	2100	44.3
V2051 Oph	...	08:54:18	70.0	30	2100	44.7
V436 Cen	2008-05-13	00:54:22	70.0	30	2100	44.4
V436 Cen	...	01:57:41	70.0	30	2100	44.9
EX Hya (Keck)	2005-02-17	12:53:57	240.0	4	960	13.4
EX Hya	2008-05-12	06:03:27	25.0	36	900	21.4
EX Hya	2008-06-21	02:00:42	25.0	36	900	20.9
VW Hyi	2008-08-22	09:02:42	25.0	36	900	19.5
VW Hyi	...	09:32:45	25.0	36	900	19.5
Z Cha	2008-05-10	23:31:41	50.0	36	1800	33.3
Z Cha	2008-09-17	09:12:36	50.0	36	1800	33.4
WX Hyi	2008-06-21	08:47:54	40.0	36	1440	27.7
WX Hyi	...	09:42:22	40.0	36	1440	27.5
V893 Sco	2008-05-10	06:39:43	40.0	36	1440	27.3
V893 Sco	2008-05-12	06:52:35	40.0	36	1440	27.2
RZ Leo (Keck)	2007-03-05	12:21:43	240.0	12	2880	44.6
TY PsA	2008-06-20	06:59:29	70.0	30	2100	33.3
TY PsA	...	08:04:50	70.0	30	2100	33.3
LHS 427	2008-07-18	02:34:55	8.0	64	512	...
LHS 427	...	02:55:00	8.0	64	512	...
LHS 2347	2008-06-26	23:46:17	30.0	30	900	...
LHS 2347	2008-07-17	23:21:52	30.0	30	900	...
LHS 3003	2008-06-20	04:17:11	10.0	56	560	...
LHS 3003	...	03:35:16	10.0	56	560	...

Note. — All objects were observed at the VLT Antu telescope using ISAAC with the exception of RZ Leo & one observation of EX Hya as described in the text. ISAAC observations required two wavelength center positions to cover the red half of the K -band, 2.25 & 2.35 μm , whereas the Keck observations required only a single setting centered at 2.21 μm .

Table 2. Program Object Observed Properties

System	$P_{\text{orb}}^{\text{a}}$ (hrs)	Primary Mass ^a (M_{\odot})	Secondary Mass ^a (M_{\odot})	Inclination ^a (degrees)	Magnitude (m_{k})	$(J - H)_{2\text{MASS}}$	$(H - K)_{2\text{MASS}}$
V2051 Oph	1.4982	0.78 ±0.06	0.15±0.03	83 ±2	13.530	0.46±0.05	0.34±0.06
V436 Cen	1.5000	0.7 ±0.1	0.17	65 ±5	13.526	0.36±0.04	0.33±0.05
EX Hya	1.6376	0.790±0.026	0.108±0.008	77.8±0.4	11.69	0.32±0.03	0.26±0.03
VW Hyi	1.7825	0.67 ±0.22	0.11 ±0.03	...	11.702	0.49±0.03	0.34±0.03
Z Cha	1.7880	0.84 ±0.09	0.125±0.014	81.1±0.14	13.314	0.40±0.05	0.25±0.05
WX Hyi	1.7955	0.9 ±0.3	0.16 ±0.05	40 ±10	12.961	0.67±0.17	0.28±0.23
V893 Sco	1.8231	0.89	0.17	72.5	12.68	0.24±0.03	0.28±0.04
RZ Leo	1.8249	15.387	0.31±0.03	0.23±0.04
TY PsA	2.02	13.583	0.42±0.05	0.29±0.05
LHS 427	6.734
LHS 2347	12.038
LHS 3003	8.928

^aCV data were taken from Ritter & Kolb (2003, update 7.12, and references therein)

Table 3. Derived Spectral Types of Program Objects.

System	Derived Spectral Type	Published Spectral Type
V2051 Oph	M7	...
V436 Cen	M8	...
EX Hya	M5	M5-M6 ^a
VW Hyi	M4	L0 ^b
Z Cha	M5	M5.5 ^c
RZ Leo	M4	M5 ^d
WX Hyi
V893 Sco	> M6	...
TY PsA	> M6	...

Note. — Estimated uncertainty is ± 1 spectral type for our determinations.

^aBeuermann & Reinsch 2008

^bMennickent et al. 2004

^cWade & Horne 1988

^dMennickent & Diaz 2002

Table 4. CO Absorption Strength Across All CV Subtypes

Star	Subtype	P_{orb} (hrs)	CO Ab. ^a	Ref ^b
Pre-CV Systems				
P83l-57	Pre-CV	...	Y	11
HS1136	Pre-CV	20.1	ND	8
RE 1016-053	Pre-CV	18.9	Y	11
UZ Sex	Pre-CV	14.3	Y	11
EC 12477-1738	Pre-CV	13.7:	Y	11
V471 Tau	Pre-CV	12.5	Y	8
EC 13349-3237	Pre-CV	11.4:	Y	11
EC 14329-1625	Pre-CV	8.4:	Y	11
BPM 6502	Pre-CV	8.08	Y	11
RR Cae	Pre-CV	7.29	Y	11
CC Cet	Pre-CV	6.82	Y	11
SDSS0743	Pre-CV	4.6	Y	8
BPM 71214	Pre-CV	4.33	Y	11
BPM 71213	Pre-CV	4.33	Y	8
EC 13471-1258	Pre-CV	3.62	Y	11
LTT 560	Pre-CV	3.54	Y	11
SDSS0757	Pre-CV	3.5	Y	8
NN Ser	Pre-CV	3.12	Y	11
SDSS0830	Pre-CV	2.9	Y	8
Non-Magnetic Systems				
EY Cyg	DN UG	11.0	W ^c	9
BT Mon	NL SW	7.99	ND	8
SY Cnc	DN ZC	9.12	ND*	5
RU Peg	DN UG	8.99	W	5
CH UMa	DN UG	8.23	W	5
MU Cen	DN UG	8.21	W	5
AC Cnc	NL SW	7.21	Y ?	5

Table 4—Continued

Star	Subtype	P_{orb} (hrs)	CO Ab. ^a	Ref ^b
EM Cyg	DN ZC	6.98	W**	5
V426 Oph	DN ZC	6.85	Y	5
SS Cyg	DN UG	6.60	W	5
AH Her	DN ZC	6.20	W	5
BV Pup	DN UG	6.35	ND	5
EX Dra	DN UG	5.04	Y	4
TW Vir	DN UG	4.38	N	4
SS Aur	DN UG	4.38	Y	8
U Gem	DN UG	4.25	W ^d	4
UU Aql	NL SW	3.92	N	4
IP Peg	DN UG	3.80	Y	4
RR Pic	NL Nb SW	3.48	W	4
TY PsA	DN SU	2.02	ND	10
RZ Leo	DN SU	1.82	Y	8
V893 Sco	DN SU	1.82	?	10
WX Hyi	DN SU	1.80	ND	10
Z Cha	DN SU	1.79	W	10
VW Hyi	DN SU	1.78	Y	10
VY Aqr	DN SU WZ	1.51	N	1
V436 Cen	DN SU	1.50	Y	10
V2051 Oph	DN SU	1.50	Y	10
WZ Sge	DN SU WZ	1.35	E	6
GW Lib	DN SU WZ ZZ	1.33	?	8
EI Psc	DN SU	1.07	N ^e	1
Magnetic Systems				
GK Per	DN Na IP	47.9	W	3
AE Aqr	NL DQ	9.86	W ^f	7
V1309 Ori	NL AM	7.98	W ^g	8
MQ Dra	NL AM LA	4.39	Y	3
SDSS0837	NL AM LA	3.18	Y	8

Table 4—Continued

Star	Subtype	P_{orb} (hrs)	CO Ab. ^a	Ref ^b
AM Her	NL AM	3.09	Y	4
AR UMa	NL AM	1.93	Y	3
ST LMi	NL AM	1.91	Y	3,8
MR Ser	NL AM	1.89	Y	4
VV Pup	NL AM	1.67	Y	2,3
EX Hya	NL IP	1.64	Y	10

Note. — Only objects with NIR observations in the K -band with $R \gtrsim 1500$ are included. A colon next to the orbital period indicates an uncertain result.

^aY=appears normal for spectral type; W=appears weaker than normal for spectral type; N=not present, but should have been for spectral type; ND=not detectable; ?=too low S/N; E=emission.

^b(1) Harrison et al. 2009, (2) Howell et al. 2006, (3) Harrison et al. 2005a, (4) Harrison et al. 2005b, (5) Harrison et al. 2004b, (6) Howell et al. 2004, (7) Harrison et al. 2007, (8) Howell et al. 2010, (9) Harrison 2010b, (10) This Work (11) Tappert et al. 2007

^cSion et al. (2004); Gänsicke et al. (2003)

^dLong & Gilliland (1999)

^eGänsicke et al. (2003)

^fJameson et al. (1980)

^gSzkody & Silber (1996); Schmidt & Stockman (2001)

*Very early spectral type, G1.5V so CO bands are not prominent

**3rd light contamination in the system, see North et al. (2000).